Sea-surface temperature records of Termination 1 in the Gulf of California: Challenges for seasonal and interannual analogues of tropical Pacific climate change

Erin L. McClymont,[1,2] Raja S. Ganeshram,[3] Laetitia E. Pichevin,[3] Helen M. Talbot,[4] Bart E. van Dongen,[5] Robert C. Thunell,[6] Alan M. Haywood,[7] Joy S. Singarayer,[8] and Paul J. Valdes[8]

Received 23 September 2011; revised 20 February 2012; accepted 20 February 2012; published 6 April 2012.

[1] Centennial-scale records of sea-surface temperature and opal composition spanning the Last Glacial Maximum and Termination 1 (circa 25–6 ka) are presented here from Guaymas Basin in the Gulf of California. Through the application of two organic geochemistry proxies, the $U^{K'}_{37}$ index and the TEX^{H}_{86} index, we present evidence for rapid, stepped changes in temperatures during deglaciation. These occur in both temperature proxies at 13 ka (~3°C increase in 270 years), 10.0 ka (~2°C decrease over ~250 years) and at 8.2 ka (3°C increase in <200 years). An additional rapid warming step is also observed in TEX^{H}_{86} at 11.5 ka. In comparing the two temperature proxies and opal content, we consider the potential for upwelling intensity to be recorded and link this millennial-scale variability to shifting Intertropical Convergence Zone position and variations in the strength of the Subtropical High. The onset of the deglacial warming from 17 to 18 ka is comparable to a "southern hemisphere" signal, although the opal record mimics the ice-rafting events of the north Atlantic (Heinrich events). Neither the modern seasonal cycle nor El Niño/Southern Oscillation patterns provide valid analogues for the trends we observe in comparison with other regional records. Fully coupled climate model simulations confirm this result, and in combination we question whether the seasonal or interannual climate variations of the modern climate are valid analogues for the glacial and deglacial tropical Pacific.

Citation: McClymont, E. L., R. S. Ganeshram, L. E. Pichevin, H. M. Talbot, B. E. van Dongen, R. C. Thunell, A. M. Haywood, J. S. Singarayer, and P. J. Valdes (2012), Sea-surface temperature records of Termination 1 in the Gulf of California: Challenges for seasonal and interannual analogues of tropical Pacific climate change, *Paleoceanography*, *27*, PA2202, doi:10.1029/2011PA002226.

1. Introduction

[2] The transitions from glacial to interglacial states (terminations) are important intervals for understanding the sensitivity of the global climate system to changing boundary conditions. The high-latitudes record dramatic climate signals during the last glacial maximum (LGM) and the most recent deglaciation (Termination 1, T1, circa 19–10 ka) [*Barker et al.*, 2009; *Denton et al.*, 2010; *Wolff et al.*, 2009]. Recent evidence shows that the tropics were also dynamic on millennial timescales [*Leduc et al.*, 2009; *Pena et al.*, 2008; *Prange et al.*, 2010]. Tropical Pacific climate is sensitive to high-latitude events via the atmosphere, through pressure systems and Intertropical Convergence Zone (ITCZ) position, and/or via the oceans, through transport of Subantarctic Mode Water in the Equatorial Undercurrent (EUC) and the presence of both Antarctic Intermediate Water (AAIW) and North Pacific Intermediate Water (NPIW) at depth [*Tsuchiya et al.*, 1989]. A sensitive response to orbital precession also offers the possibility that tropical climate variability may be somewhat independent of high-latitude forcing [*Clement et al.*, 2004]. The observed glacial-interglacial and millennial-scale tropical Pacific climate signals have used modern analogues to guide interpretation, focusing either on the modern seasonal (ITCZ migration) [*Leduc et al.*, 2009] or interannual cycles (El Niño/Southern Oscillation (ENSO)) [*Koutavas et al.*,

[1]School of Geography, Politics and Sociology, Newcastle University, Newcastle upon Tyne, UK.
[2]Department of Geography, University of Durham, Durham, UK.
[3]School of GeoSciences, Grant Institute, University of Edinburgh, Edinburgh, UK.
[4]School of Civil Engineering and Geosciences, Newcastle University, Newcastle upon Tyne, UK.
[5]School of Earth, Atmospheric and Environmental Sciences and Williamson Research Centre for Molecular Environmental Science, University of Manchester, Manchester, UK.
[6]Department of Earth and Ocean Sciences, University of South Carolina, Columbia, South Carolina, USA.
[7]School of Earth and Environment, University of Leeds, Leeds, UK.
[8]School of Geographical Sciences, University of Bristol, Bristol, UK.

0883-8305/12/2011PA002226

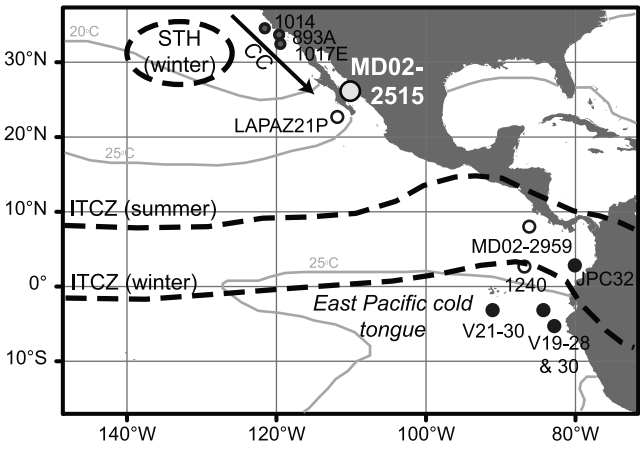

Figure 1. Location of Site MD02-2515, Guaymas Basin, Gulf of California, and selected records discussed in the text. Symbols record whether SST trends reveal a northern (late warming with cold reversals, black) or southern (early and continuous, white) hemisphere style of T1 deglaciation. California margin sites (ODP 893, 1014, 1017 [*Hendy*, 2010]) record both northern (foraminifera) and southern (alkenone) deglaciation trends in SSTs (shaded gray). Sources: LaPAZ21P [*Herbert et al.*, 2001], MD02-2959 [*Leduc et al.*, 2009], ODP 1240 [*Pena et al.*, 2008], JPC32 [*Pahnke et al.*, 2007], V21-30, V19-28 and V19-30 [*Koutavas and Sachs*, 2008]. Base map: modern mean annual SSTs from the World Ocean Atlas (2009). The approximate positions of the California Current (CC), the Subtropical High (STH(winter)) and Intertropical Convergence Zone (ITCZ) are shown.

2002; *Pena et al.*, 2008; *Prange et al.*, 2010]. Importantly, these analogues invoke different forcing mechanisms and feedbacks and thus limit our understanding of the controls over tropical Pacific climate change.

[3] Here, we exploit the climate-sensitive location of the Gulf of California (GOC) to assess the influence of high- and low-latitude forcing over tropical Pacific climate during the LGM and T1. Strong seasonal variability in SST (>15°C), biological productivity, wind strength and precipitation reflect the positions of atmospheric high pressure systems and the ITCZ, but are also modulated by ENSO [*Badan-Dangon et al.*, 1991; *Herrera-Cervantes et al.*, 2007; *Thunell*, 1998]. The GOC is aligned NW-SE, surrounded by high topography and connected to the Pacific Ocean only in the south [*Badan-Dangon et al.*, 1991]. In the winter, northwesterly winds drive upwelling and high primary production; in summer the winds weaken and there is flow of subtropical surface waters from the Pacific Ocean [*Badan-Dangon et al.*, 1991]. Subequatorial Subsurface Water and Equatorial Surface Water are upwelled during winter, and overlie NPIW [*Cheshire et al.*, 2005]. High biological productivity and low oxygen contents in bottom waters have combined to generate exceptionally well-preserved, laminated sediments [*Calvert*, 1964; *Thunell*, 1998]. Here, we present centennial-scale (~66 years) records of SSTs and marine biological productivity from IMAGES Site MD02-2515 in the Guaymas Basin, from 6 to 25 ka (Figure 1). Opal content is used as a proxy for diatom production [*Thunell*, 1998]. We utilize two temperature proxies, the $U^{K'}_{37}$ and TEX^{H}_{86} indices [*Brassell et al.*, 1986; *Kim et al.*, 2010], whose different biological origins and ecological preferences offer the potential to explore the oceanographic regime of the GOC in detail during the LGM and last deglaciation.

2. Methods

2.1. Study Site and Chronology

[4] The giant Calypso core MD02-2515 (27°29.01′N, 112°04.46′W, 881 m water depth, Figure 1) was collected from Guaymas Basin in the central GOC during the 2002 IMAGES-MONA expedition [*Beaufort et al.*, 2002]. The sediments comprise a range of terrigenous (silts and clays) and biogenic inputs (diatom ooze, nannofossils). The sediments are mostly laminated (from mm to several cm thick), with some massive and sometimes bioturbated sections. A preliminary benthic $\delta^{18}O$ age model for MD02-2515 [*Cheshire et al.*, 2005] is revised here with 13 AMS ^{14}C dates measured on bulk organic matter and selected foraminifera, converted to calendar years using the MARINE04 calibration and modern 600 year reservoir effects in the GOC (see http://calib.qub.ac.uk/calib) (Table 1) [*Reimer et al.*, 2004]. Bulk dates were necessary given limited preservation of foraminifera carbonate. We recognize that this approach introduces uncertainty given the potential for changes to the inputs and ages of terrestrial and marine organic matter inputs. However, negligible inputs of terrestrial carbon are indicated by low carbon:nitrogen ratios (~8–10), $\delta^{13}C_{org}$ (~19–21‰) and minor contributions of terrestrial lipids (e.g., from soils as discussed further below). This suggests that fossil carbon is unlikely to bias the age model shown here. The MARINE04 calibration was employed in order to ensure direct comparison with previously published data sets which used this model [e.g., *Leduc et al.*, 2009; *Pena et al.*, 2008], rather than employing the recently developed MARINE09 calibration. The assumption of a constant reservoir age is also challenging given potential variability in upwelling intensity and thus exchange with the atmosphere, as well as evidence for variable intermediate water radiocarbon content across Termination 1 [*Marchitto et al.*, 2007; *Singarayer et al.*,

Table 1. The ^{14}C AMS Dates Used to Constrain the Chronology for MD02-2515[a]

Void Corrected Core Depth (cm)	Conventional ^{14}C Age (years BP ± 1σ)	Calibrated Calendar Age (years BP)
192	6571 ± 45	6840
426	7990 ± 37	8256
631	9438 ± 40	10077
846	10517 ± 42	11293
1119	12589 ± 97	13854
1445	14767 ± 62	16894
2006	16306 ± 164	18932
2521	18383 ± 60	20988
2521*F	18397 ± 60	21007
2753	19471 ± 67	22391
2974	20972 ± 78	24365
3071	22219 ± 88	25553
3099	21994 ± 86	25303
3665	25943 ± 133	29602

[a]Radiocarbon concentrations were measured on total organic carbon and calibrated to calendar years before present (calendar years BP) using the *MARINE04* calibration and assuming a constant total reservoir correction (ΔR) of 600 years [*Reimer et al.*, 2004]. The date marked *F is a planktonic foraminifera ^{14}C AMS date.

2008] but with limited ability to correct for this. However, the variation in planktonic foraminifera ^{14}C ages shown by *Marchitto et al.* [2007] are in the order of a few hundred years, and while we acknowledge this uncertainty it is not sufficient to change the relationships with the high-latitude records which we describe below. Furthermore, we assume such effects are minimal in our records since organic matter is produced in the euphotic zone subject to atmospheric exchange. There are some minor differences in the timing of large scale features in our opal record when compared to previously published analyses from another GOC core [*Barron et al.*, 2005]. This may reflect the different age model which was applied, based on planktonic foraminifera ^{14}C and a larger ΔR [*Barron et al.*, 2005]. All ages presented here are calibrated ages in thousand-years (ka).

[5] Although the TEX_{86}^{H} index is calibrated to mean annual SST [*Kim et al.*, 2010], several studies have shown the potential for local oceanographic controls to exert a strong influence over the temperatures recorded by this proxy. Specifically, evidence has been presented which indicates the potential for TEX_{86}^{H} to record seasonal [*Wuchter et al.*, 2006] or sub-surface temperatures [*Huguet et al.*, 2007]. To test the potential impact of local processes on our down-core data set, we quantified the TEX_{86}^{H} index in eleven sediment trap samples collected between February 1996 and February 1997 at 500 m water depth in Guaymas Basin [*Thunell*, 1998]. These samples were previously analyzed for alkenones [*Goñi et al.*, 2001], which were shown to record the large seasonal cycle in SSTs but translate this into mean annual SSTs in surface sediments.

2.2. Lipid Extraction

[6] The upper 30 m (composite depth) of Core MD02-2515 was sampled at 20 cm intervals for $U_{37}^{K'}$ and TEX_{86}^{H} analyses, increased to 5 cm intervals where the benthic $\delta^{18}O$ record indicated horizons corresponding to the Last Glacial Maximum, the later stages of T1, and the earliest Holocene (composite depths 183–422 cm, 667–1105 cm, and 2554–3033 cm) [*Cheshire et al.*, 2005]. This represents an average sampling resolution of ~66 years (range 5–200 years). Samples were freeze-dried, homogenized, and extracted with dichloromethane and methanol (3:1, v:v) using microwave-assisted extraction [*Kornilova and Rosell-Melé*, 2003]. Known concentrations of *n*-tetracontane (>98%, Sigma 87096) and 1, 2-di-O-hexadecyl-*rac*-glycerol (99%, Sigma D8020) were added as internal standards. Extracts were hydrolyzed using 8% KOH in methanol, heated for 1 h at 70°C and left overnight. Neutral fractions were recovered using repeated liquid extraction with hexane. Target lipid structures are illustrated in Figure S1 in the auxiliary material.[1]

2.3. The $U_{37}^{K'}$ Index

[7] An aliquot of the neutral fraction was derivatized using bis(trimethylsilyl)trifluoroacetamide (Sigma Aldrich), and analyzed using a gas chromatograph fitted with a flame ionization detector (GC-FID) and a GC split/splitless injector (280°C) linked to a mass spectrometer (GC-MS). In both cases, separation was achieved on a fused silica capillary column (30 m × 0.25 mm i.d) coated with 0.25um dimethyl polysiloxane (HP-1MS) phase, with helium (GC) or hydrogen (GC-MS) as the carrier gas, and the following oven temperature program: 60–200°C at 20°C/min, 200–320°C at 6°C/min, and held at 310°C for 35 min. The GC-MS was operated in full scan mode (50–650 amu/sec, electron voltage 70 eV, source temperature 230°C). Lipid concentrations were calculated with reference to the internal standard (*n*-tetracontane). The $U_{37}^{K'}$ index was calculated according to the relative concentrations of the di- and tri-unsaturated C_{37} alkenones [*Prahl and Wakeham*, 1987]:

$$U_{37}^{K'} = [C_{37:2}]/[C_{37:2} + C_{37:3}] \quad (1)$$

Sea-surface temperatures (SSTs) were calculated using the global mean annual sea-surface (0 m water depth) temperature calibration [*Müller et al.*, 1998]:

$$SST(°C) = \left(U_{37}^{K'} - 0.044\right)/0.033 \quad (2)$$

Replicate extraction and analysis of selected samples determined that the average analytical reproducibility of this procedure is ±0.6°C.

2.4. The TEX_{86}^{H} and BIT Indices

[8] An aliquot of the neutral fraction was dissolved in a mixture of hexane and iso-propanol (99:1, v:v) and filtered through 0.45 mm PFTE filters. The target compounds, isoprenoid and branched glycerol diether glycerol tetraethers (GDGTs) in the trap samples were analyzed on an Agilent 1200 HPLC coupled to an Agilent 6130 quadrupole MS, while the core sediments were analyzed on a ThermoFinnigan LCQ MS. In both cases the GDGTs were analyzed by normal-phase LC-MS using a Grace Prevail Cyano HPLC column (3 μm, > 150 mm × 2.1 mm i.d.) and a guard column of the same material. Separation was achieved at 30°C with a flow rate of 0.2 mL min^{-1} and the following gradient profile: 1% isopropanol (IPA) in hexane (0–5 min); 1.8% IPA in hexane (at 25 min); 10% IPA in hexane at 30 min (hold 10 min). The ThermoFinnigan LCQ MS was equipped with an atmospheric pressure chemical ionization interface (APCI) source operated in positive ion mode. LC/MS settings were as follows: Vaporizer 400°C, capillary temperature 200°C, discharge current 5 μA, sheath gas flow 40 and auxiliary gas 6 (arbitrary units). Detection was achieved using four mass ranges, the first two between 0 and 10 min and the second pair for the remainder of the run: *m/z* 536–546 (for the internal standard, 1,2-di-O-hexadecyl-*rac*-glycerol) and *m/z* 649–659 (for archaeol), then *m/z* 1280–1310 (for isoprenoid GDGTs) and *m/z* 1015–1055 (for branched GDGTs). The Agilent MS was equipped with a multimode source operated in APCI positive ion mode. LC/MS settings were as follows: nebulizer pressure 20 psig, vaporizer temperature 250°C, drying gas (N_2) flow 6 L/min and temperature 200°C, capillary voltage 2 kV and corona 5 μA. In order to increase sensitivity/reproducibility ion scanning was performed in single ion monitoring (SIM) mode targeted to the masses of interest.

[9] The TEX_{86}^{H} index records the relative concentrations of the isoprenoid with 1 (GDGT-1), 2 (GDGT-2), and 3 (GDGT-3) cyclopentane moieties, respectively, and the crenarchaeol regio-isomer, cren' (Figure S1) [*Kim et al.*,

[1]Auxiliary materials are available in the HTML. doi:10.1029/2011PA002226.

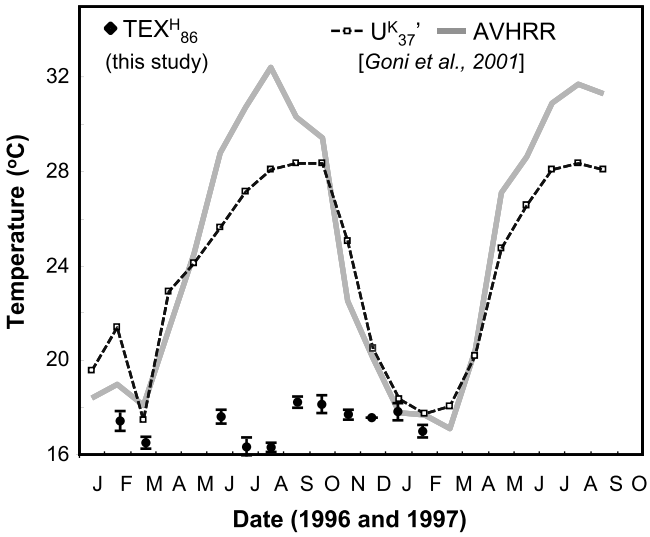

Figure 2. Guaymas Basin sediment trap temperature records. New TEX^{H}_{86} results (this study) are compared to satellite-measured (AVHRR) and published $U^{K'}_{37}$ results [*Goñi et al.*, 2001; *Thunell*, 1998]. Both TEX^{H}_{86} and $U^{K'}_{37}$ indices are calibrated to absolute temperatures using the mean annual SST calibrations discussed in the text. The sediment trap sits at 500 m water depth, around 200 m above the seafloor and in the oxygen minimum zone [*Thunell*, 1998].

2010]. The TEX^{H}_{86} index revises the original TEX_{86} index [*Schouten et al.*, 2002] for sediments outside the polar regions [*Kim et al.*, 2010]:

$$TEX^{H}_{86} = \log([\text{GDGT-2} + \text{GDGT-3} + \text{cren'}] / [\text{GDGT-1} + \text{GDGT-2} + \text{GDGT-3} + \text{cren'}]) \quad (3)$$

Temperatures were calculated using a mean annual surface (0 m water depth) temperature calibration [*Kim et al.*, 2010]:

$$SST = 68.4 \times TEX^{H}_{86} + 38.6 \quad (4)$$

Reproducibility, determined from replicate extraction and analysis of selected samples and repeated analysis of a TEX^{H}_{86} standard, was ± 0.6°C.

[10] The BIT index (Branched and Isoprenoid Tetraether Index) is a measure of the relative input to marine sediments of branched GDGTs from soil bacteria [*Hopmans et al.*, 2004]. The BIT index was calculated according to the relative concentrations of the branched GDGTs with 4 (Branched GDGT-1), 5 (branched GDGT-2) and 6 (branched GDGT-3) methyl moieties (Figure S1), respectively, and crenarchaeol (cren), following the method of *Hopmans et al.* [2004]:

$$BIT = [\text{branched GDGTs } 1 + 2 + 3] / [\text{branched GDGTs } 1 + 2 + 3 + \text{cren}] \quad (5)$$

It has recently been proposed that the absolute concentrations of branched GDGTs may be more suitable for inferring terrigenous GDGT inputs to marine sediments [*Fietz et al.*, 2011]. Branched GDGT concentrations were calculated according to the relative responses of the target lipids and the internal standard of known concentration.

2.5. Opal Content

[11] The biogenic silica component of MD02-2515 was determined at 5 cm intervals throughout the core following the method of *Mortlock and Froelich* [1989]. After alkaline extraction (2 N Na_2CO_3 solution at 85°C for 3 h), molybdate-blue spectrophotometry quantified SiOPAL, which was in turn converted to %opal using the following equation:

$$\%\ \text{opal} = \text{SiOPAL} \times 2.4 \quad (6)$$

where 2.4 is the conversion factor assuming that most of the diatomaceous silica has a relatively constant water mass of about 10% [*Mortlock and Froelich*, 1989].

2.6. Climate Modeling

[12] The fully coupled atmosphere–ocean climate model HadCM3 was used to simulate LGM and Pre-Industrial climates, and to test the impacts of freshwater hosing on the North Atlantic. The simulations shown here form part of the ensemble presented by *Singarayer and Valdes* [2010], and the model is well-documented in detail elsewhere [e.g., *Gordon et al.*, 2000]. Orbital parameters, atmospheric greenhouse gas concentrations, and ice sheet extent were prescribed [*Berger and Loutre*, 1991; *Parrenin et al.*, 2007; *Peltier*, 2004; *Petit et al.*, 1999; *Spahni et al.*, 2005]. Each simulation ran for approximately 500 years and mean climatologies are averages of the last 30 years of the simulation. An idealized hosing of the North Atlantic Ocean with freshwater was used to simulate Heinrich event 1. This was achieved by continuously adding 1 Sv of freshwater to the surface layer of the ocean model in the Atlantic between 50°N and 70°N latitude for 200 years as a continuation from an initial equilibrium simulation for 17 kyr. The magnitude and duration of freshwater inputs are poorly known, so the simulation is idealized but the forcing is typical of many previous studies [e.g., *Hewitt et al.*, 2006] and was chosen partly to ensure the shutdown of NADW formation. We emphasize here that the models are not used for direct data-model comparisons. Rather, we reflect on the patterns and signs of change as shown in the model as a reference to test and support the interpretation of our data.

3. Results

3.1. Sediment Trap TEX^{H}_{86}

[13] From February 1996 to February 1997, TEX^{H}_{86} values range from 0.48 to 0.62 (Figure 2). Using the *Kim et al.* [2010] calibration (equation (4)) these values correspond to temperatures of 16–18°C. There is no clear seasonal trend, with relatively cool temperatures recorded in June/July, and warmer temperatures recorded from September to January.

3.2. MD02-2515 Temperature and Opal Records

[14] All ages shown here are in calendar years applying the chronology outlined above and presented in Table 1. SST estimates from Site MD02-2515 across Termination 1 range between ~17.1 and 26.8°C ($U^{K'}_{37}$) and between 9.8 and 21.6°C (TEX^{H}_{86}; Figures 3a and 3b). Both temperature indices thus show a ~10°C range, with minima occurring between 17 and 18 cal. ka, and maxima reached after 8.2 cal. ka (Figures 3a and 3b). The total amplitude of warming from the 17 ka minima to the early Holocene temperatures is 7.0–

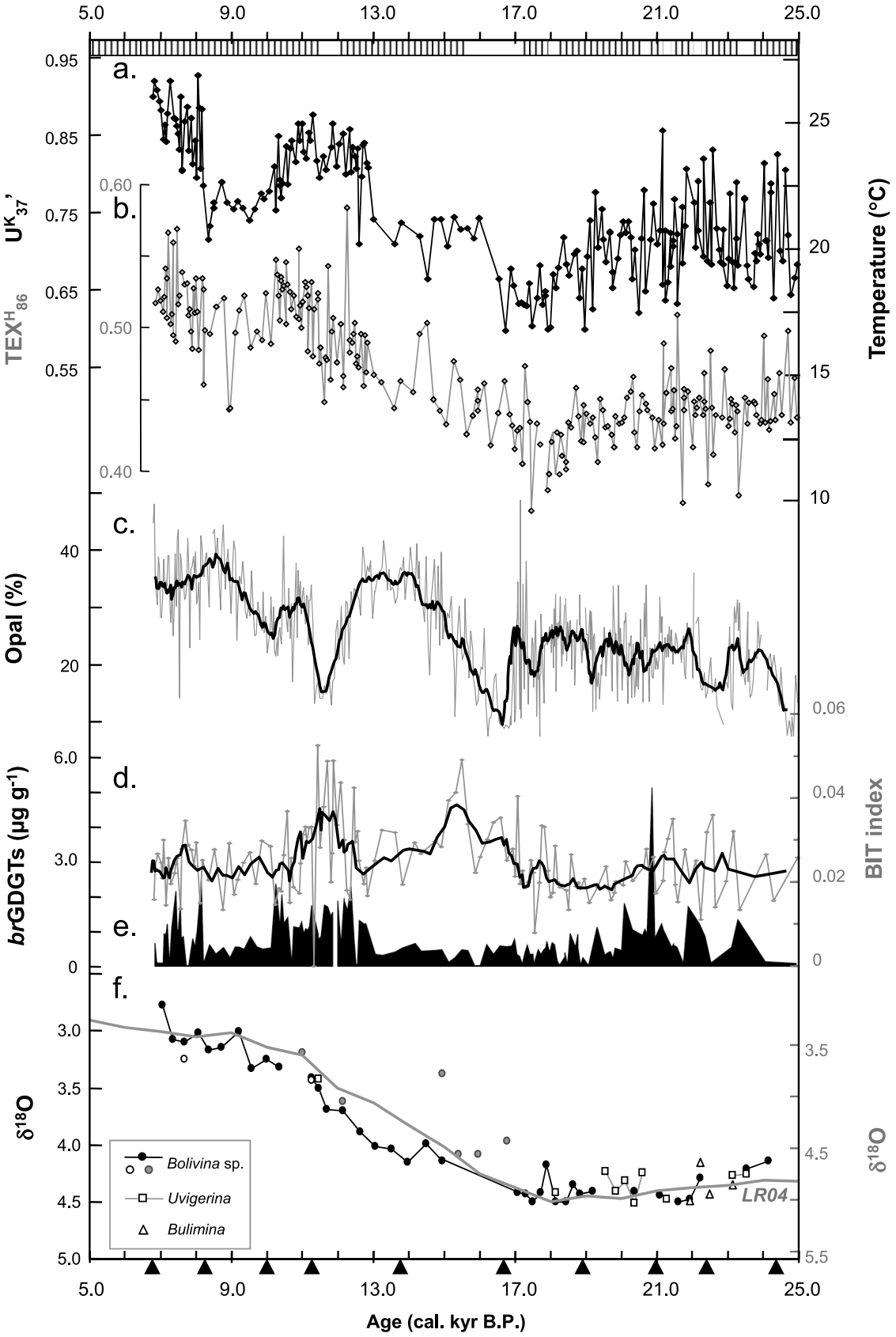
a.
b.
c.
d.
e.
f.
$U^{K'}_{37}$
TEX^{H}_{86}
Temperature (°C)
Opal (%)
brGDGTs (µg g-1)
BIT index
δ18O
Bolivina sp.
Uvigerina
Bulimina
LR04
Age (cal. kyr B.P.)

Figure 3

7.5°C. The deglacial warming is punctuated in both $U^{K'}_{37}$ and TEX^{H}_{86} indices by a series of abrupt temperature jumps, at 13 ka (2.8°C increase in 270 years), ~10.0 ka (2°C decrease over ~250 years) and at 8.2 ka (4.4°C increase in <200 years). An additional rapid warming step is also observed in TEX^{H}_{86} at 11.5 ka (2.5°C in <200 years). Between these events, plateaux in mean SSTs are observed that have ~1500 year duration i.e., between 13 and 11.5 cal. ka (warm) and 11.5 and 10 cal. ka (warming TEX^{H}_{86}), 10 and 8.2 cal. ka (cool) and from 8.2 cal. ka (warm). There is a suggestion of cooling or a temperature plateau between 14.5 and 13 cal. ka, but confirming this is limited by our relatively lower sampling resolution here (>200 years). Although the timing and magnitude of the deglacial temperature trends are replicated by the two temperature proxies, in all samples $U^{K'}_{37}$-SSTs exceed TEX^{H}_{86}-SSTs by up to 9°C.

[15] The opal content of MD02-2515 ranges from 7 to 49%, with large and high frequency variability shown throughout (Figure 3c). Before ~17.6 cal. ka opal content ranges between 10 and 30%, and between 20 and 45% after 10.7 cal. ka. Between 10.7 and 17.6 cal. ka two large cycles in opal content are observed, ranging from 10 to 40% with two minima recorded at ~11.5 and ~16.5 cal. ka. Previous work had identified two times of low opal content in the GOC across T1 but assigned the lower of these to "glacial" times [*Pride et al.*, 1999]. Our results show that the earliest interval of low opal was in fact part of the Termination. The intervals of low opal coincide with two minor increases in the BIT index, to ~0.05 (Figure 3d). Elsewhere the BIT index is extremely low, recording values of 0.010–0.025. Branched GDGT concentrations increase during the youngest interval of high BIT index values (~11.5 ka), but are low during the earlier interval (~16.5 ka; Figure 3e). The latter interval is marked by low concentrations of all GDGTs, both for branched GDGTs (<0.5 $\mu g\ g^{-1}$) and crenarchaeol (<0.5 $\mu g\ g^{-1}$). The onsets of the low opal / increased BIT intervals occur alongside temperature increases at ~17 ka ($U^{K'}_{37}$ and TEX^{H}_{86}) and at ~11.5 ka (TEX^{H}_{86} only). These also coincide with the bioturbated sediment horizons, which interrupt an otherwise-laminated sediment sequence (Figure 3).

4. Discussion

4.1. Temperature Proxy Validation

[16] We utilize two proxies with different biological origins and sensitivities to the large seasonal SST cycle in Guaymas Basin to reconstruct oceanographic changes in the GOC. The $U^{K'}_{37}$ index quantifies the relative distribution of alkenones produced by Haptophyte algae [*Prahl and Wakeham*, 1987], whereas the TEX^{H}_{86} index records the relative distributions of isoprenoidal GDGTs produced by marine Group 1 Crenarchaeota [*Kim et al.*, 2010], the latter recently re-named as Thaumarchaeota [*Brochier-Armanet et al.*, 2008]. Both proxies are calibrated to mean annual SSTs [*Kim et al.*, 2010; *Müller et al.*, 1998]. However, in sediment traps from Guaymas Basin we show that TEX^{H}_{86} is insensitive to the large seasonal SST cycle (Figure 2). The calculated temperatures (16–18°C) are in the range of present-day winter SSTs or those at the base of the thermocline [*Robinson*, 1973], where maximum Crenarchaeota abundance has been recorded [*Beman et al.*, 2008]. Conversely, $U^{K'}_{37}$ in the same sediment traps closely tracks seasonal SST changes [*Goñi et al.*, 2001].

[17] Several factors might account for the absence of the seasonal SST cycle in the GOC TEX^{H}_{86} record. Although concern has been expressed about the interference of soil GDGTs on the temperature sensitivity of TEX_{86} [*Weijers et al.*, 2006], this cannot explain the GOC results given extremely low (<0.05) BIT values. Alternatively, the recorded absolute SSTs (16–18°C) may indicate that TEX^{H}_{86} records winter temperatures in the GOC, when upwelling is at its most intense and the upper 250 m of the water column is well-mixed and at ~14–17°C [*Robinson*, 1973]. This does not, however, account for the summer TEX^{H}_{86} temperatures which exceed those of the winter SST. The third possibility is that TEX^{H}_{86} is recording temperatures well below the sea-surface, particularly in the zone below the thermocline (i.e., below ~50 m water depth) where temperatures are relatively stable at 16–18°C [*Robinson*, 1973]. Peaks in Crenarchaeota 16S rRNA gene copies have been determined below 50 m in the GOC [*Beman et al.*, 2008], supporting this interpretation. Thus, in contrast to research demonstrating the potential for a strong seasonal signal to be recorded in TEX^{H}_{86} [*Wuchter et al.*, 2006], the GOC sediment traps support evidence that TEX^{H}_{86} may record subsurface temperatures in some settings, as also shown by *Huguet et al.* [2007] in the Santa Barbara Basin and by *Lopes dos Santos et al.* [2010] in the east tropical Atlantic.

[18] As indicators of surface ($U^{K'}_{37}$) and subsurface (TEX^{H}_{86}) temperatures, the offset between the two proxies in the GOC can be explained through variations to the relative strengths of the winter upwelling and summer stratification. By comparing the two temperature proxies changes in the strength of the GOC seasonal upwelling/stratification cycle can be recorded. A well-mixed water column will raise the thermocline, reducing the $U^{K'}_{37}$-TEX^{H}_{86} temperature difference (as in winter), whereas a large difference is expected during times of stratification (summer and/or El Niño events). Thus, enhanced upwelling and a well-mixed water column will act to reduce the temperature difference between these two proxies. To record this difference through time in our downcore record, we adopt the notation ΔT, which is calculated as $SST_{UK'37}$ minus SST_{TEXH86}, using mean annual SST calibrations [cf. *Lopes dos Santos et al.*, 2010].

Figure 3. Temperature, opal content and BIT time series from Site MD02-2515, in the context of core sedimentology and chronology. Horizons used for radiocarbon dating are noted by triangles along the time axis. The presence of laminated and bioturbated horizons are marked along the upper *x* axis by vertical shading or white boxes, respectively, based on core descriptions [*Beaufort et al.*, 2002]. Absolute temperature values are shown on the right *y* axis using the calibrations detailed in the text and an inferred surface ($U^{K'}_{37}$) and subsurface (TEX^{H}_{86}) origin. (a) $U^{K'}_{37}$ index, (b) TEX^{H}_{86} index, (c) opal content, (d) BIT index, (e) branched GDGT concentrations, and (f) benthic foraminifera $\delta^{18}O$ measurements on selected species for MD02-2515 [*Cheshire et al.*, 2005], compared to the global $\delta^{18}O$ stack [*Lisiecki and Raymo*, 2005] shown in the gray line.

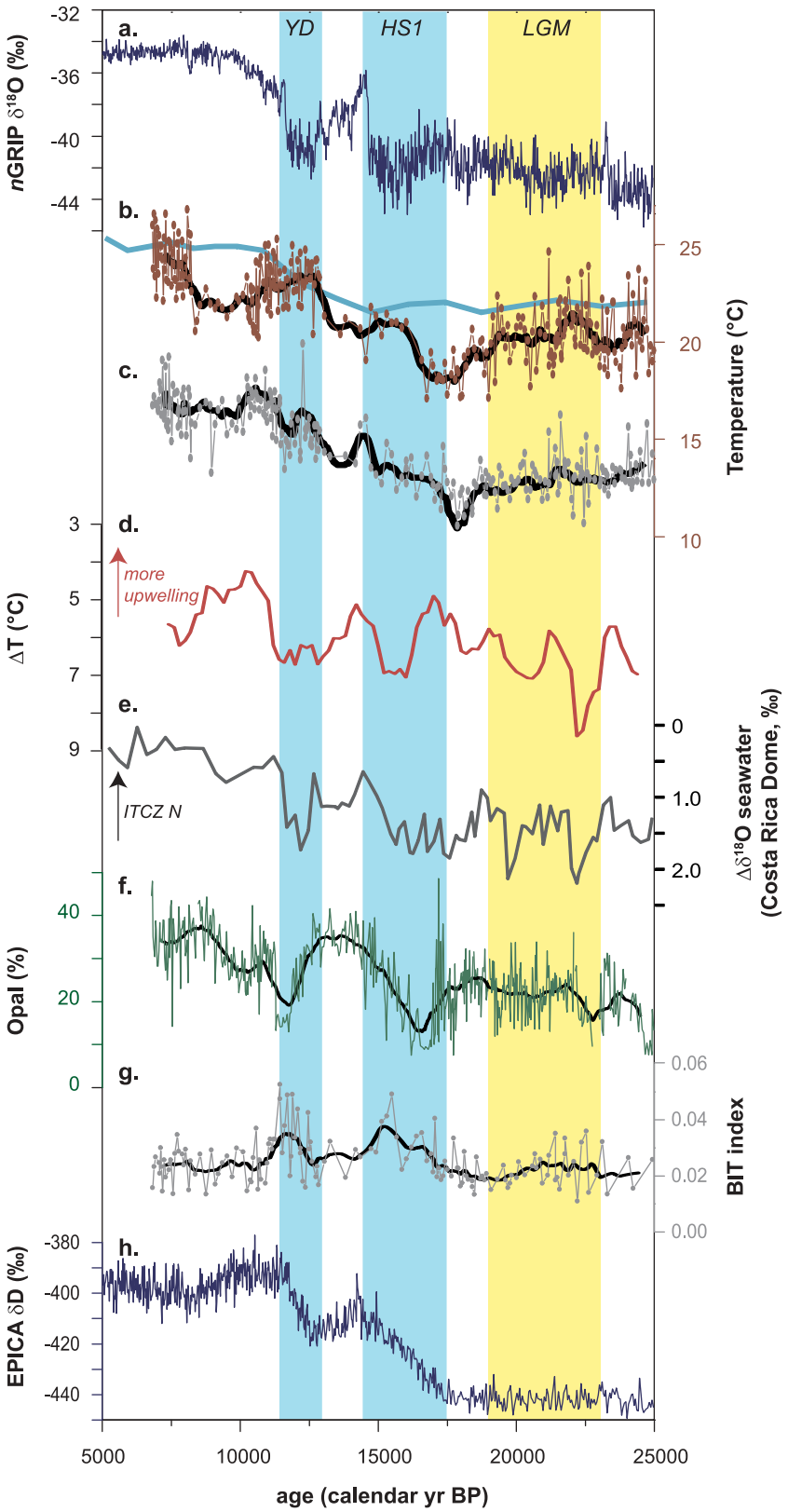
a.
b.
c.
d.
e.
f.
g.
h.
YD
HS1
LGM
nGRIP δ18O (‰)
-32
-36
-40
-44
Temperature (°C)
25
20
15
10
ΔT (°C)
3
5
7
9
more upwelling
ITCZ N
Δδ18O seawater (Costa Rica Dome, ‰)
0
1.0
2.0
Opal (%)
40
20
0
BIT index
0.06
0.04
0.02
0.00
EPICA δD (‰)
-380
-400
-420
-440
5000
10000
15000
20000
25000
age (calendar yr BP)

Figure 4

4.2. Circulation History in the GOC Across the LGM and T1

[19] Both temperature proxies reveal a 10°C range across the interval of study, with minima occurring between 17 and 18 cal. ka (Figures 3a and 3b). Absolute temperatures from $U^{K'}_{37}$ and TEX^{H}_{86} temperature are offset during the LGM and T1, and the resulting temperature difference (ΔT) contains millennial-scale variability with a ~4–8°C range (Figure 4d). Using the EPILOG definition of the LGM (19–23 cal kyr) [*Mix et al.*, 2001], the mean LGM $SST_{UK'37}$ of 21°C (range 18–24°C) gives an approximate anomaly relative to present of −3.5°C. This is at the upper range of the −2 to −3°C SST anomaly for the northeast tropical Pacific presented by the MARGO synthesis [*MARGO Project Members*, 2009], but within 1.0°C of the closest MARGO data point at LAPAZ-21P (Figure 1) [*Herbert et al.*, 2001; *MARGO Project Members*, 2009]. Large fluctuations in SST occur at millennial- and centennial-scales, ±1°C for T1 and the early Holocene, increased to ±2°C for the LGM (Figure 3a). Given that each 1 cm sediment slice analyzed here represents around 5 years, this variability is entirely consistent with the range of modern interannual anomalies in mean annual SSTs driven by ENSO [*Herrera-Cervantes et al.*, 2007; *Lavín et al.*, 2003].

[20] *Cheshire et al.* [2005] argued that during glacial times, a weaker and more southerly position of the Subtropical High in response to the presence of the Laurentide ice sheet would have limited the influence of winter winds in the GOC and thus reduced upwelling and its associated biological productivity. Overall, glacial stage opal contents are lower than during the early Holocene, supporting a weaker upwelling influence, but there is still considerable millennial-scale variability in both opal content and ΔT which indicate times of variable upwelling intensity during the LGM (Figures 4d and 4f). This may reflect a more dynamic Subtropical High and/or ITCZ position during the LGM than previously considered, superimposed upon an overall southward shift of both systems under glacial conditions.

[21] The onset of the deglacial warming in the GOC from 17 to 18 ka lags the early warming observed in some sites from the California borderlands region (from ~22–25 ka [*Herbert et al.*, 2001; *Lyle et al.*, 2010]) and from the equatorial Pacific (from ~20 ka, [*Pena et al.*, 2008]), but leads SST increases recorded in the Santa Barbara Basin [*Hendy*, 2010], offshore Baja California [*Herbert et al.*, 2001], and in the equatorial Pacific cold tongue [*Koutavas et al.*, 2002]. In contrast to the California Current System and east equatorial Pacific cold tongue [*Hendy*, 2010; *Koutavas and Sachs*, 2008], there is no clear response to the abrupt deglacial cooling events in the North Atlantic, Heinrich 1 (H1, ~17.5–14.6 ka) and the Younger Dryas (YD, ~12.8–11.5 ka, [*Denton et al.*, 2010]). Rather, there is warming from 17 to 18 ka, which is subdued or reversed around 14 ka, before warming resumes from circa 13 ka. This temperature trend across T1 more closely resembles the "southern hemisphere" continuous warming pattern of the EPICA δD record (Figure 4h), as also observed in the equatorial Pacific [*Leduc et al.*, 2009; *Pena et al.*, 2008] and Peru margin [*Lamy et al.*, 2004]. Our extremely high-resolution sampling reveals rapid warming steps which have not previously been detected for T1, of 2–3°C in less than 300 years at 13.0 and 8.2 ka. This contrasts with planktonic δ^{18}O records from the GOC [*Keigwin*, 2002], which suggest that gradual warming occurred from 15 ka, until a "suppressed cooling" marked the onset of the YD. However, such differences probably reflect the variable influence of salinity on planktonic δ^{18}O during T1, which our runoff proxies (BIT index, Figure 3d) infer had also changed. The stepped warming that we observe is also associated with rapid changes in biogenic proxies at a nearby GOC core, JPC56 [*Barron et al.*, 2005], but absolute SSTs were not reconstructed. The new data shown here thus confirm that a dynamic tropical Pacific climate system operated at millennial timescales through the LGM and T1.

[22] The temperature difference (ΔT) contains millennial-scale variability with a 4–8°C range which we interpret here to represent variations in upwelling intensity in the GOC (Figure 4d). High ΔT coincide with convergence of GOC and Baja California alkenone SSTs (Figures 4b and 4d) [*Herbert et al.*, 2001], as observed during summer in response to enhanced northward advection of warm tropical Pacific waters and suppressed GOC upwelling. In contrast, low ΔT when GOC and Baja California SSTs diverge (Figures 4b and 4d), confirms the presence of colder, upwelled waters in the GOC. Despite the "southern hemisphere" T1 temperature trend overall, GOC opal content records two rapid declines in diatom production centered on 15.5 and 11.5 ka (Figures 3c and 4e). The association of low opal, convergence of GOC-Baja California SSTs, high ΔT, and enhanced runoff (BIT index) is analogous to modern summer and/or El Niño events in the GOC [*Lavín et al.*, 2003; *Thunell*, 1998]. These conditions coincide with the H1 and YD stadials detailed above, The low-opal intervals coincide with high magnetic susceptibility, titanium and carbonate contents in MD02-2515 [*Cheshire et al.*, 2005], and low opal horizons in other GOC cores [*Barron et al.*, 2005], previously inferred to represent higher precipitation and lower upwelling-driven biological production in the basin. Branched GDGT concentrations do not increase during HS1, suggesting that the higher BIT index may in part reflect reduced contributions of crenarchaeol, as considered by *Fietz et al.* [2011]. However, reduced crenarchaeota production is consistent with the overall decline in primary productivity and upwelling strength as indicated by other

Figure 4. MD02-2515 results compared to east Pacific and high-latitude climate records. One thousand year running means for the MD02-2515 data are shown by solid black lines. (a) Greenland temperatures (nGRIP δ^{18}O [*Andersen et al.*, 2006]). (b) $U^{K'}_{37}$ index SSTs from MD02-2515 (red, this study) and Baja California (blue, Site LAPAZ-21P [*Herbert et al.*, 2001]). (c) TEX^{H}_{86} index subsurface temperatures from MD02-2515 (this study). (d) Guaymas Basin temperature difference (ΔT = $SST_{UK'37}$ minus SST_{TEXH86}, using 1000 year running means for both proxies). (e) $\Delta\delta^{18}O_{sw}$, an expression of sea-surface salinity in the Costa Rica Dome (MD02-2529 [*Leduc et al.*, 2009]). (f) Guaymas Basin percent opal (this study). (g) Guaymas Basin BIT index (this study). (h) Antarctic temperatures (EPICA δD [*Jouzel et al.*, 2007]). The LGM, Heinrich 1 (H1) and Younger Dryas (YD) stadials are defined as by *Denton et al.* [2010].

proxies. Reduced winter bloom diatom species and increased tropical- or ENSO-related diatoms in GOC core JPC56 also support an increased presence of subtropical waters during these intervals [*Barron et al.*, 2005; *Pride et al.*, 1999; *Sancetta*, 1995]. A recent study also suggests that the availability of micronutrients such as Fe can affect opal records in this setting [*Pichevin et al.*, 2012]. The presence of bioturbated sediments at these times in MD02-2515 (Figure 3) highlights the presence of oxygen in the bottom waters of the GOC, which likely reflect reduced production and respiration as upwelling weakened.

[23] High opal contents, comparable to Holocene and modern surface sediments [*Douglas et al.*, 2007], are first identified from 15 ka. There is also a decrease in ΔT and the BIT index, both suggestive of a reduced summer mode and/or increased winter upwelling signature, although absolute SSTs do not change. Diatom and silicoflagellate remains also suggest that this time, coincident with the Bølling-Allerød, was marked by conditions similar to present in the GOC [*Barron et al.*, 2005]. This interpretation is supported by our alkenone SSTs, which lie only 1–2°C below the modern annual mean at this time (Figures 3a and 4b).

[24] The early Holocene at MD02-2515 is marked by a pronounced and sustained decrease in SSTs (10.5–8.2 ka) that interrupts the overall deglacial warming trend. This is accompanied by the lowest recorded ΔT (4–5°C), increased opal content, and divergence of the GOC and Baja SSTs (Figure 4). These patterns suggest an intensification of upwelling at the onset of the Holocene, consistent with diatom assemblages indicating stronger winter winds [*Sancetta*, 1995]. At 8.2 ka, a rapid and large increase in $SST_{UK'37}$ occurs (3°C increase in <200 years). Opal contents continue to remain high, and ΔT returns to values experienced through the LGM and T1. The GOC and Baja California $SST_{UK'37}$ records also converge once more, suggesting either an increasing influence of the summer mode of circulation and/or a reduction in upwelling intensity and duration.

4.3. Regional Implications: Low- or High-Latitude Forcing?

[25] The overall SST increases in the GOC across T1 lead those observed in the Greenland ice sheet (Figure 4a) but are more closely related in time and shape to those recorded in the EPICA ice core (Figure 4h) and other sites which record a "southern hemisphere" warming signal [*Leduc et al.*, 2009; *Pena et al.*, 2008; *Lamy et al.*, 2004]. Given that the GOC is an upwelling regime, fed by subsurface and intermediate waters sourced outside the region, a remote forcing via changes in the temperature of these water masses is a distinct possibility. Benthic foraminifera $\delta^{18}O$ has been used to infer a 4°C cooling in intermediate waters of the Pacific during the LGM including those of the SW Pacific and NPIW [*Herguera et al.*, 2010; *Stott et al.*, 2007]. In the Santa Barbara Basin, these temperature signals could be observed in both surface and intermediate waters with gradual warming developing from 17 ka and a larger and abrupt warming at 14.7 ka [*Hendy and Kennett*, 2003; *Hendy*, 2010]. Such evolution in intermediate water temperatures might also explain the links between the temperature trends of the GOC and Peruvian margin [*Lamy et al.*, 2004]. Thus, although there is similarity in the timing and magnitude of intermediate water temperature changes compared to GOC SSTs, this relationship is complex.

[26] Several studies in this region have linked local upwelling intensity to atmospheric circulation strength which may (through the Subtropical High) have been linked to the presence of the Laurentide ice sheet [e.g., *Cheshire et al.*, 2005; *Ganeshram and Pedersen*, 1998]. The coincidence of low opal content and high ΔT (weakened upwelling) during times of north Atlantic ice-rafting (Figure 4) raise the possibility that surface warming might also reflect reduced upwelling strength, and thus be connected to the northern hemisphere. This is broadly supported by similarity between the ΔT and opal records showing two minima during the deglacial roughly during the H1 and YD events. However, the relationship between ΔT and opal content is not always perfect. For instance, the opal minima occur well after the ΔT decline during the YD. This may suggest that the opal records are also affected by factors other than upwelling, including micronutrient availability [*Pichevin et al.*, 2012].

[27] There remains disagreement over whether modern analogues based on seasonal [*Leduc et al.*, 2009] and/or interannual [*Pena et al.*, 2008; *Prange et al.*, 2010] climate variability are appropriate as a guide for understanding the processes operating during glacial and deglacial tropical Pacific climates. This is important since they involve quite different forcing and feedback processes. Low GOC ΔT (more upwelling) correlates to low sea-surface salinity in the Costa Rica Dome (Site MD02-2529, Figure 4e), argued to reflect northward displacement of the ITCZ during Greenland interstadials [*Leduc et al.*, 2009]. This is the opposite relationship between GOC upwelling and ITCZ position in the modern seasonal cycle, and is particularly pronounced during the H1 and YD stadials when "summer" circulation is indicated for the GOC but the Costa Rice Dome record would propose that the ITCZ was shifted to the south [*Leduc et al.*, 2009]. This challenge to the modern GOC-ITCZ analogue is maintained until circa 11.5 ka, when the modern relationship is re-established (lower GOC ΔT and increased salinity in the Costa Rica Dome, Figures 4d and 4e). It has been hypothesized that a weaker Subtropical High in response to the Laurentide ice sheet [*Ganeshram and Pedersen*, 1998] restricted upwelling-favorable winds in the GOC to summer/interstadials [*Cheshire et al.*, 2005], thus reversing the modern GOC/ITCZ relationship. Model simulations also indicate the potential for reversal of the seasonal cycle of east Pacific cold tongue emergence in response to altered inter-hemispheric temperature gradients [*Chiang et al.*, 2008], such as those which occurred during Greenland stadials when Antarctica warmed [*Wolff et al.*, 2009]. Studies of the sensitivity of tropical Pacific circulation to extra-tropical forcing, and in particular to changes in inter-hemispheric temperature gradients, have also shown that while the ITCZ tends to migrate to the warmer hemisphere (i.e., south during times of northern hemisphere cooling), this could have a southern hemisphere origin via changes to the strength of convection, the southerlies, and the emergence of the east Pacific cold tongue [*Chiang et al.*, 2008; *Kang et al.*, 2008]. Thus, the southern hemisphere may play a more active role in the millennial-scale variability in the tropical Pacific than has been considered, as

well as influencing the overall warming trend of the glacial-interglacial transition.

[28] Furthermore, the interpretation of the Costa Rica Dome salinity record as a reflection of ITCZ position has been questioned recently [*Prange et al.*, 2010]. This alternative explanation draws on the regional hydrological impact of changing the strength of the Choco Jet (which transports moisture from the Atlantic to the Pacific over Central America [*Poveda and Mesa*, 2000]). This reconciles evidence for a northward position of the Pacific ITCZ during north Atlantic ice-rafting events, as recorded in SSTs, primary productivity and rainfall [*Kienast et al.*, 2006; *Koutavas and Sachs*, 2008; *Pahnke et al.*, 2007], by using ENSO as an analogue [*Prange et al.*, 2010]. It is also argued that the ENSO analogue can account for the southward shift of the Atlantic ITCZ [*Peterson et al.*, 2000] but northward shift in the Pacific ITCZ during the H1 and YD stadials, since this is observed at present during La Niña events [*Prange et al.*, 2010]. Although the GOC record presented here supports the notion of a northward shift of the ITCZ during the H1 and YD stadials, the use of ENSO as an analogue to explain the GOC patterns (warm SSTs, low productivity, high rainfall) would argue for an "El Niño"-like situation for the H1 and YD stadials. This conflicts with the "La Niña-like" circulation argued to operate at these times [*Prange et al.*, 2010], but is supported by sea-surface salinity anomalies in the west Pacific [*Stott et al.*, 2002] and zonal SST gradients [*Koutavas et al.*, 2002]. The debate surrounding the application of ENSO analogues to millennial-scale variability in the tropical Pacific is thus far from being resolved.

[29] The modern ocean/atmosphere circulation in the GOC is closely linked to the strength and position of the Subtropical High in the north Pacific, which is argued to have responded to the growth of the Laurentide ice sheet and reduced solar insolation by weakening and/or being displaced to the south [*Cheshire et al.*, 2005; *Hendy*, 2010; *Yamamoto et al.*, 2004]. For example, early deglacial warming in the California Current at the LGM has been argued to reflect an increased northward influence of subtropical waters [*Herbert et al.*, 2001] and/or reduced California Current flow [*Lyle et al.*, 2010] given a weaker Subtropical High. Millennial-scale fluctuations in SSTs in the California Current System have also been linked to north Atlantic oscillations via atmospheric circulation including changes in the strength of the Subtropical High and Aleutian Low [*Hendy*, 2010].

[30] From 21 to 16 ka, divergence between GOC and Baja California SSTs occurs (Figure 4b), and alkenone-SSTs from the California margin become anti-correlated with those of the GOC. This pattern is consistent with the proposal of a weakened and southward displacement of the Subtropical High using the modern winter mode as an analogue [*Yamamoto et al.*, 2004]. Pollen records in California and an increased north-south SST gradient along the California margin argue for a weakened, rather than a displaced, Subtropical High [*Lyle et al.*, 2010]. However, in comparing SST proxies from the California margin, *Hendy* [2010] noted that planktonic foraminifera continued to record low SSTs in contrast to the warming observed in the alkenone record from 20 ka. *Hendy* [2010] attributed this difference to a strengthening of the Subtropical High in response to increasing summer insolation from 20 ka, driving enhanced summer/autumn warmth in the California Current System (CCS; from alkenones) while the Aleutian Low remained strong and sustained cool winter conditions (planktonic foraminifera). Our data do not allow differentiation between these two mechanisms, since the GOC is sensitive to the direction as well as the strength of the wind systems, which are driven by both the position and intensity of the Subtropical High. However, there is also evidence for a northward migration of the ITCZ from 20 ka given the presence of increasingly salty and warm thermocline waters in the east equatorial Pacific, argued to reflect strengthening of the Equatorial Undercurrent [*Pena et al.*, 2008]. For either scenario, the correlations between the GOC and the CCS temperature records are difficult to reconcile using ENSO as an analogue, since opposing signs are suggested by the warm CCS ("El Niño") but strengthening EUC ("La Niña") across the Termination.

4.4. Model Simulations

[31] Neither the modern seasonal cycle in ITCZ position and Subtropical High strength nor ENSO anomalies are able to fully capture the trends and patterns observed in the GOC and the wider tropical Pacific during the LGM and T1. A suite of climate simulations for the LGM, H1 and the pre-industrial era using a global coupled ocean–atmosphere climate model (HadCM3 [*Gordon et al.*, 2000]) was performed to test whether the relationships and processes indicated by the paleo-data could also be observed independently. As outlined above (section 2.6), we do not use our model outputs for direct data-model comparison, but rather as a means of reflecting on whether the patterns and signs of change in the simulations might offer support or explanation for our data interpretation.

[32] Model outputs suggest that the Subtropical High was not displaced south during the LGM, but had enhanced summer winds in a direction which is conducive to upwelling at present (Figures 5f and 5i) and stronger winds blowing onshore during winter (Figures 5e and 5h), which would not be conducive to upwelling (see also Figure S2 for surface wind stress calculations). Thus, summer winds could have driven upwelling under glacial conditions, and might explain

Figure 5. (a–f) Model-simulated tropical Pacific wind strength and direction (absolute values) and (g–l) anomalies, both in meters per second, for key time intervals. Outputs shown by (left) annual mean, (middle) winter, and (right) summer. Summer is defined as June, July, and August; winter is defined as December, January, February. (a) Mean annual, Pre-Industrial; (b) winter, Pre-Industrial; (c) summer, Pre-Industrial; (d) mean annual, LGM; (e) winter, LGM; (f) summer, LGM; (g) mean annual anomalies, LGM-Pre-Industrial; (h) winter anomalies, LGM minus Pre-Industrial; (i) summer anomalies, LGM minus Pre-Industrial; (j) mean annual anomalies, H1 minus LGM; (k) winter anomalies, H1 minus LGM; and (l) summer anomalies, H1 minus LGM. Figures S2 and S3 show the original model outputs for mean sea level pressure and surface wind stress.

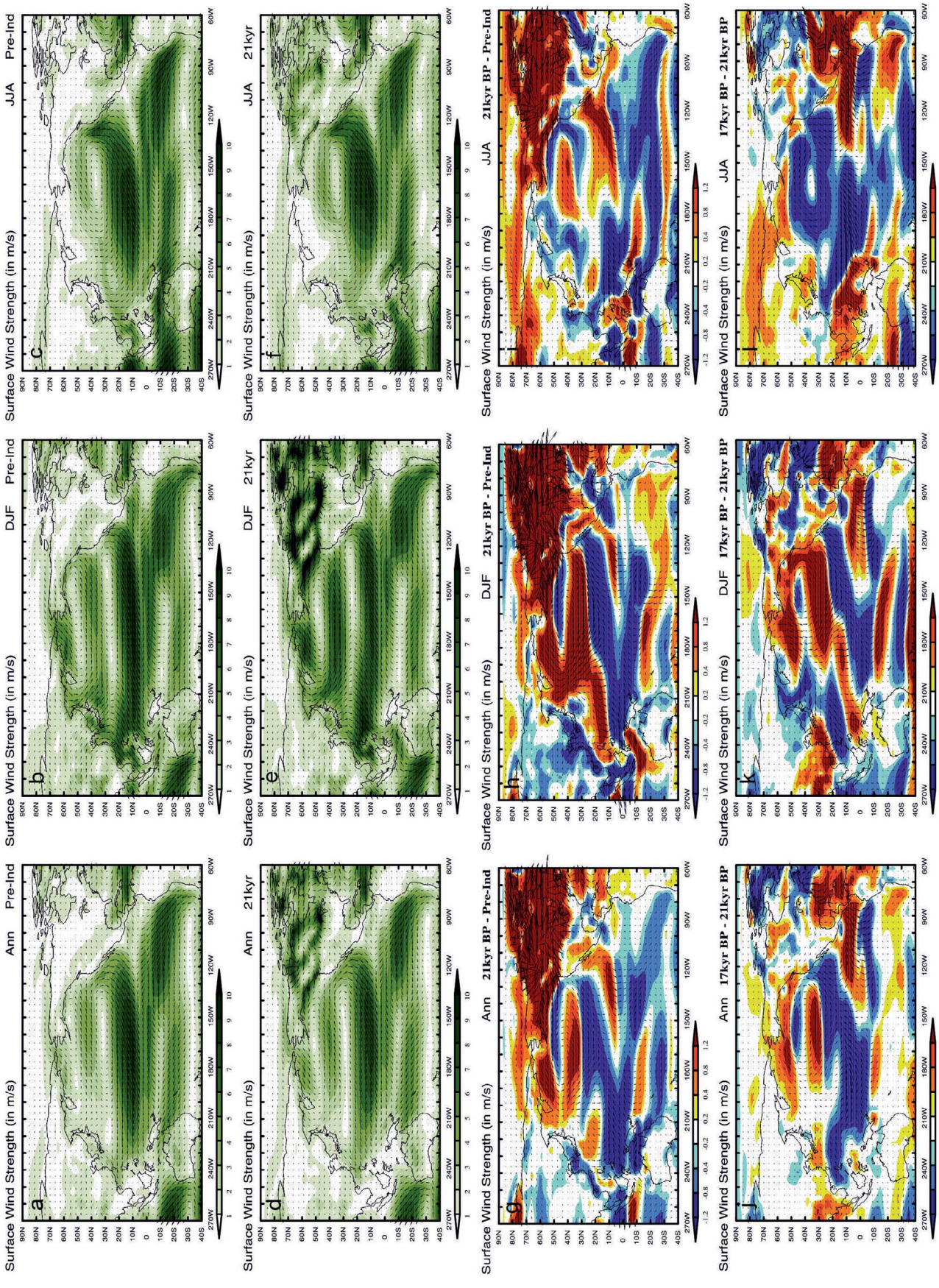
Surface Wind Strength (in m/s)
Ann
Pre-Ind
DJF
JJA
21kyr
21kyr BP - Pre-Ind
17kyr BP - 21kyr BP
a
b
c
d
e
f
g
h
i
j
k
l

Figure 5

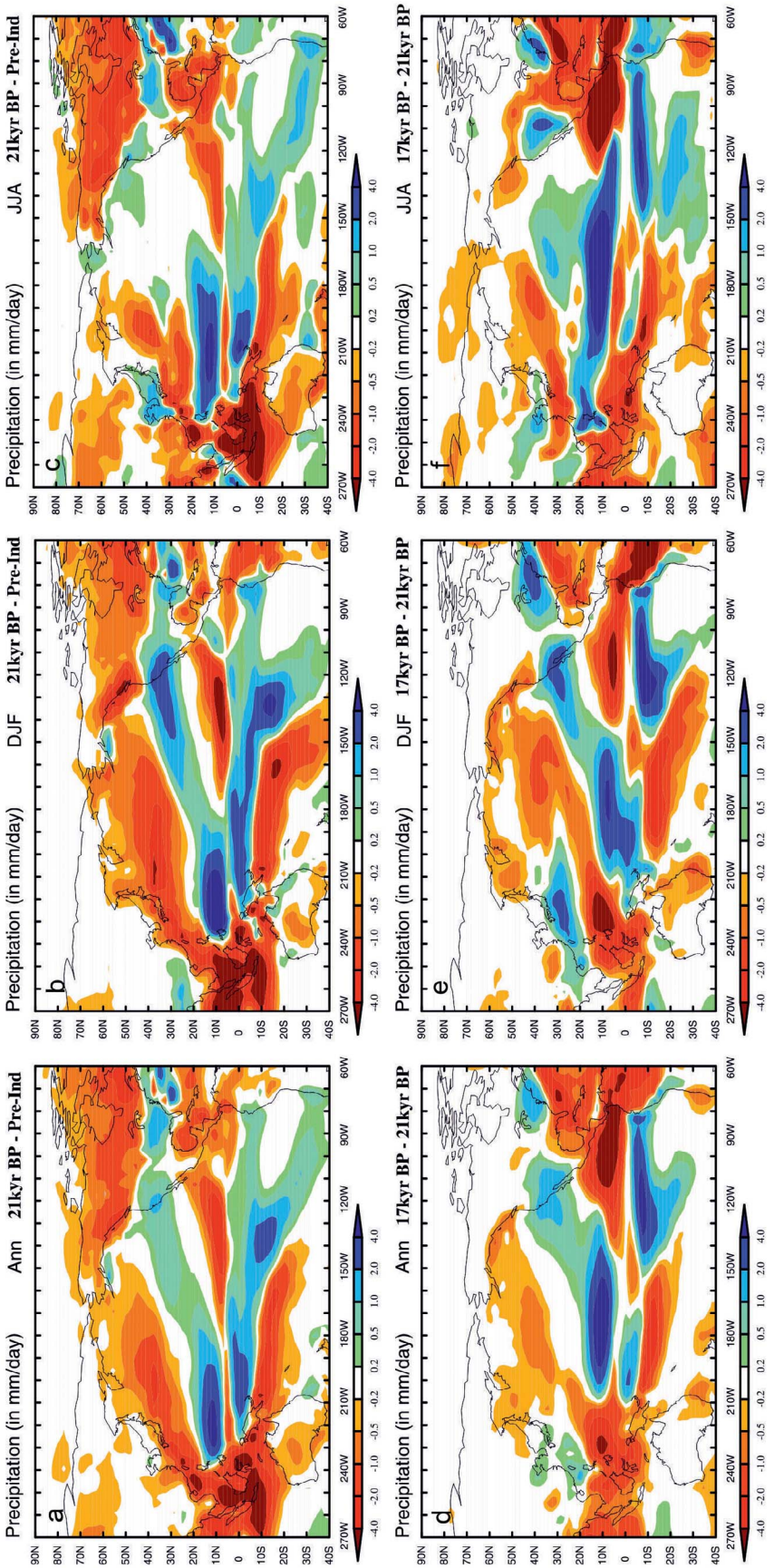

Figure 6. Model-simulated tropical Pacific precipitation rate anomalies (mm day^{-1}) for key time intervals. Outputs shown by (left) annual mean, (middle) winter, and (right) summer. Summer is defined as in Figure 5. (a) Mean annual anomalies, LGM-Pre-Industrial; (b) winter anomalies, LGM minus Pre-Industrial; (c) summer anomalies, LGM minus Pre-Industrial; (d) mean annual anomalies, H1 minus LGM; (e) winter anomalies, H1 minus LGM; and (f) summer anomalies, H1 minus LGM. Figures S2 and S3 show the original model outputs for surface wind stress and mean sea level pressure.

why upwelling increased during the "warm" conditions at millennial timescales but decreased during times of northern hemisphere cooling (the reverse of present, Figures 5b and 5c). The LGM Aleutian Low was deeper during winter at the LGM (Figure S3), which in turn enhanced the pressure gradient and thus the wind systems continued to be relatively strong. The seasonal precipitation distribution gives no indication of a shift in the ITCZ position (Figures 6a and 6c). While there is an increase in zonal temperature gradient across the Pacific at the LGM ("La Niña-like"), the distribution of precipitation anomalies relative to present instead shows an eastward migration of convection in the west Pacific, a pattern which is partly analogous to "El Niño-like" conditions. This might account for the different patterns shown by the salinity and SST proxy data.

[33] By hosing the North Atlantic with freshwater, the model generally predicts enhancement of the glacial climate anomalies in response to Heinrich events (Figures 5 and 6). Significantly, an increase in precipitation and runoff is also predicted to the north of the GOC, supported by our BIT index (Figure 3d) and terrigenous metal flux [*Cheshire et al.*, 2005]. The Aleutian Low deepens further (explaining cool northern California margin SSTs [*Hendy*, 2010], Figure S3), and a small reduction in both winter and summer wind strength on the east of the Subtropical High is suggested. The apparent collapse of upwelling in the GOC during the hosing events in the paleo-data does not entirely support the "stronger glacial" state shown by the model, but perhaps a sensitive GOC response to the precipitation / wind strength anomalies. The model outputs confirm the interpretations of our paleo-data: that neither modern seasonal nor interannual climate variability can adequately guide interpretation of the trends and relationships observed in the tropical Pacific and along the California margin during the LGM and across T1, and should be used cautiously as analogues for past climate changes.

5. Conclusions

[34] New centennial-scale records of sea-surface temperature and opal content spanning the LGM and T1 (circa 25–6 ka) were generated from a site in the GOC in order to understand the relationships between low- and high-latitude forcing of tropical Pacific climate change. Using two different organic geochemistry proxies, the $U^{K'}_{37}$ index and the TEX^{H}_{86} index, we have shown evidence for rapid, stepped changes in temperatures during deglaciation, at 13 ka, 10.0 ka and 8.2 ka. The combination of records for temperature and opal content reveal variations in upwelling intensity which can be linked to shifting ITCZ position and variations in the strength of the Subtropical High. The overall deglacial warming trend from 17 to 18 ka is comparable to a "southern hemisphere" signal, although the ΔT and opal records show evidence for a response to the ice-rafting events of the north Atlantic (Heinrich events).

[35] By determining millennial-scale variability in upwelling dynamics we have demonstrated that neither the seasonal nor interannual climates of the present-day can explain the trends observed. In part this reflects subtle but important differences in atmospheric circulation as demonstrated by our model simulations, which can result in quite different anomalies in temperature, precipitation and wind intensity as recorded in proxy data.

[36] **Acknowledgments.** We thank the following organizations for funding support: the Natural Environment Research Council (NERC) (E.L.M. (NE/E00119X/1) and R.S.G.), the Royal Society (E.L.M.), the Scottish Alliance for GeoSciences (SAGES) fellowship (R.S.G. and L.E.P.), and the Leverhulme Trust (Philip Leverhulme Prize to A.M.H. in 2008). We thank the IMAGES IV Programme and the crew and scientific party of the MONA expedition (R/V *Marion Dufresne*) for core collection. Helen Beddow, Paul Donohoe, Ian Harrison, and Paul Lythgoe are thanked for their laboratory and analytical assistance. We thank the NERC Radiocarbon laboratory at East Kilbride, U. K., and Steve Moreton for radiocarbon analysis. The Science Research Infrastructure Fund (SRIF) from HEFCE is thanked for funding the purchase of the ThermoFinnigan LCQ ion trap mass spectrometer at Newcastle University. We thank Dorothy Pak, Tom Russon, Takeshi Nakagawa, and Stewart Jamieson for their discussions and constructive comments. We also thank R. Zahn, J. D. Carriquiry, and two anonymous reviewers for their insightful comments.

References

Andersen, K. K., et al. (2006), The Greenland ice core chronology 2005, 15–42 ka. Part 1: Constructing the time scale, *Quat. Sci. Rev.*, *25*, 3246–3257, doi:10.1016/j.quascirev.2006.08.002.

Badan-Dangon, A., C. E. Dorman, M. A. Merrifield, and C. D. Wianat (1991), The lower atmosphere over the Gulf of California, *J. Geophys. Res.*, *96*(C9), 16,877–16,896, doi:10.1029/91JC01433.

Barker, S., P. Diz, M. J. Vautravers, J. Pike, G. Knorr, I. R. Hall, and W. S. Broecker (2009), Interhemispheric Atlantic seesaw response during the last deglaciation, *Nature*, *457*, 1097–1102, doi:10.1038/nature07770.

Barron, J. A., D. Bukry, and W. E. Dean (2005), Paleoceanographic history of the Guaymas Basin, Gulf of California, during the past 15,000 years based on diatoms, silicoflagellates, and biogenic sediments, *Mar. Micropaleontol.*, *56*, 81–102, doi:10.1016/j.marmicro.2005.04.001.

Beaufort, L., et al. (2002), Cruise report MD126 MONA (Marges Ouest Nord Américaines) – IMAGESVIII, 452 pp., Inst. Polaire Fr. Paul-Emile Victor, Plouzaneé, France.

Beman, J. M., B. N. Popp, and C. A. Francis (2008), Molecular and biogeochemical evidence for ammonia oxidation by marine Crenarchaeota in the Gulf of California, *ISME J.*, *2*, 429–441, doi:410.1038/ismej.2007.118.

Berger, A., and M. F. Loutre (1991), Insolation values for the climate of the last 10 million years, *Quat. Sci. Rev.*, *10*, 297–317, doi:10.1016/0277-3791(91)90033-Q.

Brassell, S. C., G. Eglinton, I. T. Marlowe, U. Pflaumann, and M. Sarnthein (1986), Molecular stratigraphy: A new tool for climatic assessment, *Nature*, *320*, 129–133, doi:10.1038/320129a0.

Brochier-Armanet, C., B. Boussau, S. Gribaldo, and P. Forterre (2008), Mesophilic Crenarchaeota: Proposal for a third archaeal phylum, the Thaumarchaeota, *Nat. Rev. Microbiol.*, *6*, 245–252, doi:10.1038/nrmicro1852.

Calvert, S. E. (1964), Factors affecting distribution of laminated diatomaceous sediments in Gulf of California, in *Marine Geology of the Gulf of California*, edited by T. H. van Andel and G. G. Shor, *Mem. Am. Assoc. Pet. Geol.*, *3*, 311–330.

Cheshire, H., J. Thurow, and A. J. Nederbragt (2005), Late Quaternary climate change record from two long sediment cores from Guaymas Basin, Gulf of California, *J. Quat. Sci.*, *20*, 457–469, doi:10.1002/jqs.944.

Chiang, J. C. H., Y. Fang, and P. Chang (2008), Interhemispheric thermal gradient and tropical Pacific climate, *Geophys. Res. Lett.*, *35*, L14704, doi:10.1029/2008GL034166.

Clement, A. C., A. Hall, and A. J. Broccoli (2004), The importance of precessional signals in the tropical climate, *Clim. Dyn.*, *22*, 327–341, doi:10.1007/s00382-003-0375-8.

Denton, G. H., R. F. Anderson, J. R. Toggweiler, R. L. Edwards, J. M. Schaefer, and A. E. Putnam (2010), The last glacial termination, *Science*, *328*, 1652–1656, doi:10.1126/science.1184119.

Douglas, R., O. Gonzalez-Yajimovich, J. Ledesma-Vazquez, and F. Staines-Urias (2007), Climate forcing, primary production and the distribution of Holocene biogenic sediments in the Gulf of California, *Quat. Sci. Rev.*, *26*, 115–129, doi:10.1016/j.quascirev.2006.05.003.

Fietz, S., A. Martínez-Garcia, C. Huguet, G. Rueda, and A. Rosell-Melé (2011), Constraints in the application of the Branched and Isoprenoid Tetraether index as a terrestrial input proxy, *J. Geophys. Res.*, *116*, C10032, doi:10.1029/2011JC007062.

Ganeshram, R. S., and T. F. Pedersen (1998), Glacial-interglacial variability in upwelling and bioproductivity off NW Mexico: Implications for Quaternary paleoclimate, *Paleoceanography*, *13*, 634–645, doi:10.1029/98PA02508.

Goñi, M. A., D. M. Hartz, R. C. Thunell, and E. Tappa (2001), Oceanographic considerations for the application of the alkenone-based

paleotemperature $U^{K'}_{37}$ index in the Gulf of California, *Geochim. Cosmochim. Acta*, *65*, 545–557, doi:10.1016/S0016-7037(00)00559-7.

Gordon, C., C. Cooper, C. A. Senior, H. Banks, J. M. Gregory, T. C. Johns, J. F. B. Mitchell, and R. A. Wood (2000), The simulation of SST, sea ice extents and ocean heat transports in a version of the Hadley Centre coupled model without flux adjustments, *Clim. Dyn.*, *16*, 147–168, doi:10.1007/s003820050010.

Hendy, I. L. (2010), The paleoclimatic response of the Southern Californian Margin to the rapid climate change of the last 60 ka: A regional overview, *Quat. Int.*, *215*, 62–73, doi:10.1016/j.quaint.2009.06.009.

Hendy, I. L., and J. P. Kennett (2003), Tropical forcing of North Pacific intermediate water distribution during Late Quaternary rapid climate change?, *Quat. Sci. Rev.*, *22*, 673–689, doi:10.1016/S0277-3791(02)00186-5.

Herbert, T. D., J. D. Schuffert, D. Andreasen, L. Heusser, M. Lyle, A. Mix, A. C. Ravelo, L. D. Stott, and J. C. Herguera (2001), Collapse of the California Current during glacial maxima linked to climate change on land, *Science*, *293*, 71–76, doi:10.1126/science.1059209.

Herguera, J. C., T. Herbert, M. Kashgarian, and C. Charles (2010), Intermediate and deep water mass distribution in the Pacific during the Last Glacial Maximum inferred from oxygen and carbon stable isotopes, *Quat. Sci. Rev.*, *29*, 1228–1245, doi:10.1016/j.quascirev.2010.02.009.

Herrera-Cervantes, H., D. B. Lluch-Cota, S. E. Lluch-Cota, and G. Gutiérrez-de-Velasco S (2007), The ENSO signature in sea-surface temperature in the Gulf of California, *J. Mar. Res.*, *65*, 589–605, doi:10.1357/002224007783649529.

Hewitt, C. D., A. J. Broccoli, M. Crucifix, J. M. Gregory, J. F. B. Mitchell, and R. J. Stouffer (2006), The effect of a large freshwater perturbation on the glacial North Atlantic Ocean using a coupled general circulation model, *J. Clim.*, *19*, 4436–4447, doi:10.1175/JCLI3867.1.

Hopmans, E. C., J. W. H. Weijers, E. Schefuß, L. Herfort, J. S. Sinninghe Damsté, and S. Schouten (2004), A novel proxy for terrestrial organic matter in sediments based on branched and isoprenoid tetraether lipids, *Earth Planet. Sci. Lett.*, *224*, 107–116, doi:10.1016/j.epsl.2004.05.012.

Huguet, C., A. Schimmelmann, R. Thunell, L. J. Lourens, J. S. Sinninghe Damsté, and S. Schouten (2007), A study of the TEX_{86} paleothermometer in the water column and sediments of the Santa Barbara Basin, California, *Paleoceanography*, *22*, PA3203, doi:10.1029/2006PA001310.

Jouzel, J., et al. (2007), Orbital and millennial Antarctic climate variability over the past 800,000 years, *Science*, *317*, 793–796, doi:10.1126/science.1141038.

Kang, S. M., I. M. Held, D. M. W. Frierson, and M. Zhao (2008), The response of the ITCZ to extratropical thermal forcing: Idealized slab-ocean experiments with a GCM, *J. Clim.*, *21*, 3521–3532, doi:10.1175/2007JCLI2146.1.

Keigwin, L. D. (2002), Late Pleistocene-Holocene paleoceanography and ventilation of the Gulf of California, *J. Oceanogr.*, *58*, 421–432, doi:10.1023/A:1015830313175.

Kienast, M., S. S. Kienast, S. E. Calvert, T. I. Eglinton, G. Mollenhauer, R. François, and A. C. Mix (2006), Eastern Pacific cooling and Atlantic overturning circulation during the last deglaciation, *Nature*, *443*, 846–849.

Kim, J.-H., J. van der Meer, S. Schouten, P. Helmke, V. Willmott, F. Sangiorgi, N. Koç, E. C. Hopmans, and J. S. Sinninghe Damsté (2010), New indices and calibrations derived from the distribution of crenarchaeal isoprenoid tetraether lipids: Implications for past sea surface temperature reconstructions, *Geochim. Cosmochim. Acta*, *74*, 4639–4654.

Kornilova, O., and A. Rosell-Melé (2003), Application of microwave-assisted extraction to the analysis of biomarker climate proxies in marine sediments, *Org. Geochem.*, *34*, 1517–1523, doi:10.1016/S0146-6380(03)00155-4.

Koutavas, A., and J. P. Sachs (2008), Northern timing of deglaciation in the eastern equatorial Pacific from alkenone paleothermometry, *Paleoceanography*, *23*, PA4205, doi:10.1029/2008PA001593.

Koutavas, A., J. Lynch-Stieglitz, T. M. Marchitto Jr., and J. P. Sachs (2002), El Niño-like pattern in ice age tropical Pacific sea surface temperature, *Science*, *297*, 226–230, doi:10.1126/science.1072376.

Lamy, F., J. Kaiser, U. Ninnemann, D. Hebbeln, H. W. Arz, and J. Stoner (2004), Antarctic timing of surface water changes off Chile and Patagonian ice sheet response, *Science*, *304*, 1959–1962, doi:10.1126/science.1097863.

Lavín, M. F., E. Palacios-Hernández, and C. Cabrera (2003), Sea surface temperature anomalies in the Gulf of California, *Geofis. Int.*, *42*, 363–375.

Leduc, G., L. Vidal, K. Tachikawa, and E. Bard (2009), ITCZ rather than ENSO signature for abrupt climate changes across the tropical Pacific?, *Quat. Res.*, *72*, 123–131, doi:10.1016/j.yqres.2009.03.006.

Lisiecki, L. E., and M. E. Raymo (2005), A Pliocene-Pleistocene stack of 57 globally distributed benthic $\delta^{18}O$ records, *Paleoceanography*, *20*, PA1003, doi:10.1029/2004PA001071.

Lopes dos Santos, R. A., M. Prange, I. S. Castañeda, E. Schefuß, S. Mulitza, M. Schulz, E. M. Niedermeyer, J. S. Sinninghe Damsté, and S. Schouten (2010), Glacial–interglacial variability in Atlantic meridional overturning circulation and thermocline adjustments in the tropical North Atlantic, *Earth Planet. Sci. Lett.*, *300*, 407–414, doi:10.1016/j.epsl.2010.10.030.

Lyle, M., L. Heusser, C. Ravelo, D. Andreasen, A. Olivarez Lyle, and N. Diffenbaugh (2010), Pleistocene water cycle and eastern boundary current processes along the California continental margin, *Paleoceanography*, *25*, PA4211, doi:10.1029/2009PA001836.

Marchitto, T. M., S. J. Lehman, J. D. Ortiz, J. Flückiger, and A. van Geen (2007), Marine radiocarbon evidence for the mechanism of deglacial atmospheric CO_2 rise, *Science*, *316*, 1456–1459, doi:10.1126/science.1138679.

MARGO Project Members (2009), Constraints on the magnitude and patterns of ocean cooling at the Last Glacial Maximum, *Nat. Geosci.*, *2*, 127–132, doi:10.1038/ngeo411.

Mix, A. C., E. Bard, and R. Schneider (2001), Environmental processes of the ice age: Land, oceans, glaciers (EPILOG), *Quat. Sci. Rev.*, *20*, 627–657, doi:10.1016/S0277-3791(00)00145-1.

Mortlock, R. A., and P. N. Froelich (1989), A simple method for the rapid determination of biogenic opal in pelagic marine sediments, *Deep Sea Res., Part A*, *36*, 1415–1426, doi:10.1016/0198-0149(89)90092-7.

Müller, P. J., G. Kirst, G. Ruhland, I. V. Storch, and A. Rosell-Melé (1998), Calibration of the alkenone paleotemperature index $U^{K'}_{37}$ based on core-tops from the eastern South Atlantic and the global ocean (60°N–60°S), *Geochim. Cosmochim. Acta*, *62*, 1757–1772, doi:10.1016/S0016-7037(98)00097-0.

Pahnke, K., J. P. Sachs, L. Keigwin, A. Timmermann, and S.-P. Xie (2007), Eastern tropical Pacific hydrologic changes during the past 27,000 years from D/H ratios in alkenones, *Paleoceanography*, *22*, PA4214, doi:10.1029/2007PA001468.

Parrenin, F., et al. (2007), The EDC3 chronology for the EPICA dome C ice core, *Clim. Past*, *3*, 485–497, doi:10.5194/cp-3-485-2007.

Peltier, W. R. (2004), Global glacial isostasy and the surface of the ice-age Earth: The ICE-5G (VM2) Model and GRACE, *Annu. Rev. Earth Planet. Sci.*, *32*, 111–149, doi:10.1146/annurev.earth.32.082503.144359.

Pena, L. D., I. Cacho, P. Ferretti, and M. A. Hall (2008), El Niño–Southern Oscillation–like variability during glacial terminations and interlatitudinal teleconnections, *Paleoceanography*, *23*, PA3101, doi:10.1029/2008PA001620.

Peterson, L. C., G. H. Haug, K. A. Hughen, and U. Röhl (2000), Rapid changes in the hydrologic cycle of the tropical Atlantic during the last glacial, *Science*, *290*, 1947–1951, doi:10.1126/science.290.5498.1947.

Petit, J. R., et al. (1999), Climate and atmospheric history of the past 420,000 years from the Vostok ice core, Antarctica, *Nature*, *399*, 429–436, doi:10.1038/20859.

Pichevin, L. E., R. S. Ganeshram, B. Reynolds, F. G. Prahl, T. F. Pedersen, R. C. Thunell, and E. L. McClymont (2012), Silicic acid biogeochemistry in the Gulf of California: Insights from sedimentary Si isotopes, *Paleoceanography*, doi:10.1029/2011PA002237, in press.

Poveda, G., and O. J. Mesa (2000), On the existence of Lloró (the rainiest locality on Earth): Enhanced ocean-land-atmosphere interaction by a low-level jet, *Geophys. Res. Lett.*, *27*, 1675–1678.

Prahl, F. G., and S. G. Wakeham (1987), Calibration of unsaturation patterns in long-chain ketone compositions for palaeotemperature assessment, *Nature*, *330*, 367–369, doi:10.1038/330367a0.

Prange, M., S. Steph, M. Schulz, and L. D. Keigwin (2010), Inferring moisture transport across Central America: Can modern analogs of climate variability help reconcile paleosalinity records?, *Quat. Sci. Rev.*, *29*, 1317–1321, doi:10.1016/j.quascirev.2010.02.029.

Pride, C., R. Thunell, D. Sigman, L. Keigwin, M. Altabet, and E. Tappa (1999), Nitrogen isotopic variations in the Gulf of California since the Last Deglaciation: Response to global climate change, *Paleoceanography*, *14*, 397–409, doi:10.1029/1999PA900004.

Reimer, P. J., et al. (2004), IntCal04 terrestrial radiocarbon age calibration, 0–26 cal kyr BP, *Radiocarbon*, *46*, 1029–1058.

Robinson, M. K. (1973), *Atlas of Monthly Mean Sea Surface and Subsurface Temperatures in the Gulf of California*, *Mem. San Diego Soc. Nat. Hist.*, vol. 5, pp. 1–97, Soc. Nat. Hist., San Diego, Calif.

Sancetta, C. (1995), Diatoms in the Gulf of California: Seasonal flux patterns and the sediment record for the last 15,000 years, *Paleoceanography*, *10*, 67–84, doi:10.1029/94PA02796.

Schouten, S., E. C. Hopmans, E. Schefuß, and J. S. Sinninghe Damsté (2002), Distributional variations in marine crenarchaeotal membrane lipids: A new tool for reconstructing ancient sea water temperatures?, *Earth Planet. Sci. Lett.*, *204*, 265–274, doi:10.1016/S0012-821X(02)00979-2.

Singarayer, J. S., and P. J. Valdes (2010), High-latitude climate sensitivity to ice-sheet forcing over the last 120 kyr, *Quat. Sci. Rev.*, *29*, 43–55, doi:10.1016/j.quascirev.2009.10.011.

Singarayer, J. S., D. A. Richards, A. Ridgwell, P. J. Valdes, W. E. N. Austin, and J. W. Beck (2008), An oceanic origin for the increase of atmospheric radiocarbon during the Younger Dryas, *Geophys. Res. Lett.*, *35*, L14707, doi:10.1029/2008GL034074.

Spahni, R., et al. (2005), Atmospheric methane and nitrous oxide of the Late Pleistocene from Antarctic ice cores, *Science*, *310*, 1317–1321, doi:10.1126/science.1120132.

Stott, L., C. Poulsen, S. Lund, and R. Thunell (2002), Super ENSO and global climate oscillations at millennial time scales, *Science*, *297*, 222–226, doi:10.1126/science.1071627.

Stott, L., A. Timmermann, and R. Thunell (2007), Southern Hemisphere and deep-sea warming led deglacial atmospheric CO_2 rise and tropical warming, *Science*, *318*, 435–438, doi:10.1126/science.1143791.

Thunell, R. C. (1998), Seasonal and annual variability in particle fluxes in the Gulf of California: A response to climate forcing, *Deep Sea Res., Part I*, *45*, 2059–2083, doi:10.1016/S0967-0637(98)00053-3.

Tsuchiya, M., R. Lukas, R. A. Fine, E. Firing, and E. J. Lindstrom (1989), Source waters of the Pacific Equatorial undercurrent, *Prog. Oceanogr.*, *23*, 101–147, doi:10.1016/0079-6611(89)90012-8.

Weijers, J. W. H., S. Schouten, O. C. Spaargaren, and J. S. Sinninghe Damsté (2006), Occurrence and distribution of tetraether membrane in soils: Implications for the use of the TEX_{86} proxy and the BIT index, *Org. Geochem.*, *37*, 1680–1693, doi:10.1016/j.orggeochem.2006.07.018.

Wolff, E. W., H. Fischer, and R. Röthlisberger (2009), Glacial terminations as southern warmings without northern control, *Nat. Geosci.*, *2*, 206–209, doi:10.1038/ngeo442.

Wuchter, C., S. Schouten, S. G. Wakeham, and J. S. Sinninghe Damsté (2006), Archaeal tetraether membrane lipid fluxes in the northeastern Pacific and the Arabian Sea: Implications for TEX86 paleothermometry, *Paleoceanography*, *21*, PA4208, doi:10.1029/2006PA001279.

Yamamoto, M., T. Oba, J. Shimamune, and T. Ueshima (2004), Orbital-scale anti-phase variation of sea surface temperature in mid-latitude North Pacific margins during the last 145,000 years, *Geophys. Res. Lett.*, *31*, L16311, doi:10.1029/2004GL020138.

R. S. Ganeshram and L. E. Pichevin, School of GeoSciences, Grant Institute, University of Edinburgh, West Mains Road, Edinburgh EH9 3JW, UK. (r.ganeshram@ed.ac.uk; l.pichevin@ed.ac.uk)

A. M. Haywood, School of Earth and Environment, University of Leeds, Woodhouse Lane, Leeds LS2 9JT, UK. (earamh@leeds.ac.uk)

E. L. McClymont, Department of Geography, University of Durham, South Road, Durham DH1 3LE, UK. (erin.mcclymont@durham.ac.uk)

J. S. Singarayer and P. J. Valdes, School of Geographical Sciences, University of Bristol, University Road, Bristol BS8 1SS, UK. (p.j.valdes@bris.ac.uk)

H. M. Talbot, School of Civil Engineering and Geosciences, Newcastle University, Newcastle upon Tyne NE1 7RU, UK. (helen.talbot@ncl.ac.uk)

R. C. Thunell, Department of Earth and Ocean Sciences, University of South Carolina, Columbia, SC 29208, USA. (thunell@geol.sc.edu)

B. E. van Dongen, School of Earth, Atmospheric and Environmental Sciences, University of Manchester, Oxford Road, Manchester M13 9PL, UK. (bart.vandongen@manchester.ac.uk)